Accepted Manuscript

Enhancement of CO_2/CH_4 separation performances of 6FDA-based co-polyimides mixed matrix membranes embedded with UiO-66 nanoparticles

Mohd Zamidi Ahmad, Marta Navarro, Miloslav Lhotka, Beatriz Zornoza, Carlos Téllez, Vlastimil Fila, Joaquín Coronas

PII: S1383-5866(17)31928-7
DOI: https://doi.org/10.1016/j.seppur.2017.10.039
Reference: SEPPUR 14121

To appear in: *Separation and Purification Technology*

Received Date: 16 June 2017
Revised Date: 18 October 2017
Accepted Date: 18 October 2017

Please cite this article as: M. Zamidi Ahmad, M. Navarro, M. Lhotka, B. Zornoza, C. Téllez, V. Fila, J. Coronas, Enhancement of CO_2/CH_4 separation performances of 6FDA-based co-polyimides mixed matrix membranes embedded with UiO-66 nanoparticles, *Separation and Purification Technology* (2017), doi: https://doi.org/10.1016/j.seppur.2017.10.039

Enhancement of CO_2/CH_4 separation performances of 6FDA-based co-polyimides mixed matrix membranes embedded with UiO-66 nanoparticles

Mohd Zamidi Ahmad[1, 2], Marta Navarro[2], Miloslav Lhotka[1], Beatriz Zornoza[2], Carlos Téllez[2], Vlastimil Fila[1], Joaquín Coronas[2*]

[1]Department of Inorganic Technology, University of Chemistry and Technology, 16628 Prague, Czech Republic

[2]Chemical and Environmental Engineering Department and Institute of Nanoscience Aragon (INA), Universidad de Zaragoza, 50018 Zaragoza, Spain

*Corresponding author: coronas@unizar.es

Abstract

Metal-organic frameworks (MOFs) incorporation into mixed matrix membranes (MMMs) is gaining more attention due to the combined advantages of high separation performance and easy processability. Nanoparticles (NPs) of CO_2-philic MOF UiO-66 (Zr-BDC) were synthesized with high surface area and ca. 50 nm particle size (and also for comparison with 100 and 200 nm sizes). They were incorporated into three 6FDA-based co-polyimides (namely 6FDA-BisP, 6FDA-ODA, and 6FDA-DAM), forming MMMs with loadings in the 4 – 23 wt.% range. The NPs and MMMs were characterized accordingly by XRD, BET, SEM, TEM, FTIR, and TGA. CO_2 and CH_4 isotherms on the NPs were measured by a static volumetric method at the pressure up to 10 bar. Fractional free volume (FFV) was calculated using solid density, measured by pycnometer. Gas separation performance was evaluated using a feed composition of 50%:50% CO_2:CH_4 binary mixture at 35 °C and a pressure difference of 2 bar. The presence of UiO-66 NPs in the continuous 6FDA-BisP and 6FDA-ODA co-polyimides improved both CO_2 permeability and CO_2/CH_4 selectivity by 50 – 180% and 70 - 220%, respectively. In the case of 6FDA-DAM MMMs, the CO_2 permeability was significantly improved by 92%, while maintaining the CO_2/CH_4 selectivity. The best results in terms of CO_2/CH_4 selectivity were 41.9 for 6FDA-BisP (17 wt.% filler loading, 108 Barrer of CO_2), 57.0 for 6FDA-ODA (7 wt.% filler loading, 43.3 Barrer of CO_2) and 32.0 for 6FDA-DAM (8 wt.% filler loading, 1728 Barrer of CO_2). The study confirmed the UiO-66 NPs incorporation into these co-polyimides has brought the improvement of the dense membranes, without jeopardizing their positive attributes.

Keywords: Gas separation, 6FDA-based co-polyimide, Metal-organic framework, UiO-66, Mixed matrix membrane.

1. Introduction

The number of investigations on metal-organic frameworks (MOFs) has grown rapidly in the past few years due to their promising applications in gas storage and separation. The potential application varies from the eminent purpose of natural gas sweetening and CO_2 post-combustion capture to the in-house air purification. MOFs can be classified by their three-dimensional crystalline frameworks with permanent porosity, formed with metal-based clusters linked by organic ligands [1]. The infinite possibilities of metal and linker selections in the synthesis of MOFs give researchers a variety of coordination geometry choices, i.e., tetrahedral, pyramidal or bi-pyramidal, trigonal or octahedron [2]. This design flexibility allows the MOFs to be attuned to their intended purposes. Additionally, their inherent properties are remarkable advantages, such as high CO_2 uptakes (e.g. HKUST-1 of 7.32 [3] and 10.71 $mmol \cdot g^{-1}$ [4], MIL-53 of 10.02 $mmol \cdot g^{-1}$ [4], MIL-100 of 9.98 $mmol \cdot g^{-1}$ [5], MIL-101 of 7.20 $mmol \cdot g^{-1}$ [6]), open porous framework structures with large accessible pore volumes, tuneable pore affinity and most importantly their relatively high chemical and thermal stabilities. Several intensive reviews on MOFs for CO_2 separation [7–10] have been made available, and several others [1,2,11] comprehensively discussed on the MOF synthesis. The incorporation of these MOFs dispersed into the polymer continuous-phase as mixed matrix membranes (MMMs) has been reported using both low flux (e.g., PSF [12], PVAc [13] and PBI [14]) and high flux (e.g., rubbery PDMS [15] and glassy 6FDA-DAM [16,17]) polymers.

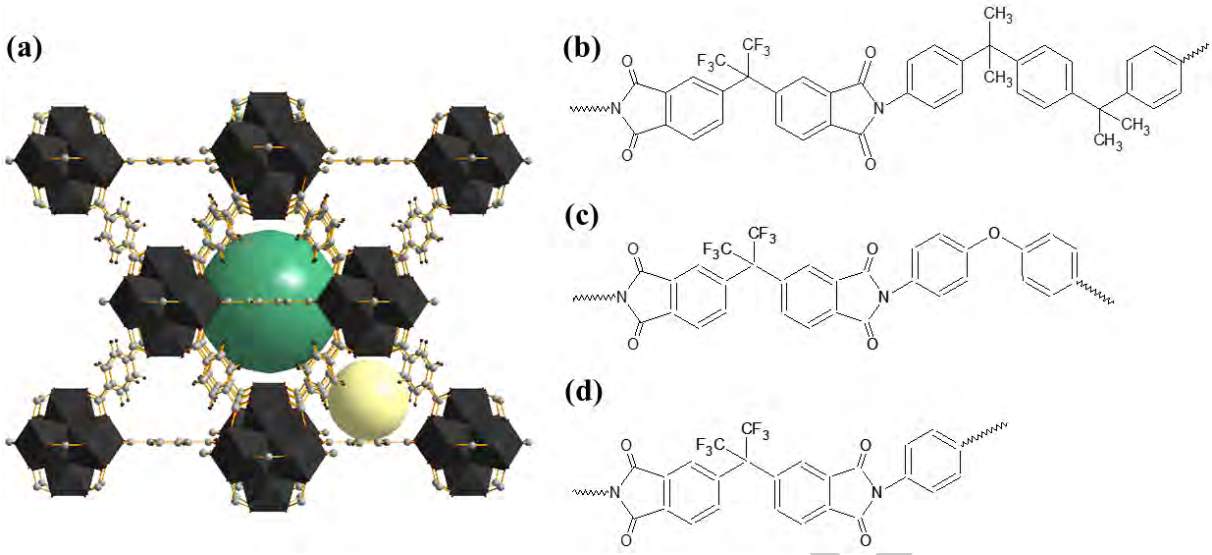

Figure 1: (a) Representation of iso-reticular UiO-66 framework with its Zr_6O_6 cuboctahedron polyhedral (dark grey) with octahedron (green ball) and tetrahedron (yellow ball) free volumes. The structure was drawn using Diamond 3.2 with CIF obtained from CDCC open database [18]. Chemical structures of 6FDA co-polyimides presented are (b) 6FDA-BisP, (c) 6FDA-ODA and (d) 6FDA-DAM.

Scientific attention towards the relatively new class of highly crystalline zirconium-based MOFs, especially UiO-66 (UiO: University of Oslo) grows rapidly. UiO-66 is based on a $Zr_6O_4(OH)_4$ octahedron, forming 12-fold lattices connected by the organic linker, 1,4-benzene-dicarboxylate (BDC) (Figure 1a) [18]. This zirconium terephthalate has high surface area, of experimental values 850 – 1300 $m^2 \cdot g^{-1}$ [12,19–21], and the theoretically accessible surface of 1021 $m^2 \cdot g^{-1}$ [22]. The microporous framework composes of centric octahedral cages (ca. 11 Å) each connects with eight corner tetrahedral cages (ca. 8 Å) by means of trigonal windows (ca. 6 Å). The crystal face-centered-cubic contributes to its high stability towards heat (reported between 430 and 540 ºC [23,24]), pressure [25], water [25,26], common solvents [25], even strong acid (HCl) and base (NaOH) [24]. The UiO-66 also possess low heat adsorption with the increase of CO_2 and CH_4 loading, due to its bulky and non-polar aromatic ring which sterically hinders the highly adsorptive metal cluster to adsorb the heat [22,27]. This is another added-value feature which is very desirable for thermal stability and lower cost regeneration.

Khdhayyer *et al.* [28] have recently published their findings regarding the incorporation of UiO-66 into the highly permeable polymer of intrinsic microporosity (PIM-1). The CO_2 permeability was increased to 7610 Barrer, obtaining a 60% improvement with 23 wt.% of UiO-66 loading. The CO_2/CH_4 selectivity, however, decreased with loading more than 9 wt.%. Castarlenas *et al.* [12] reported H_2/CH_4 and CO_2/CH_4 separation with UiO-66 MMMs, where the H_2/CH_4 selectivity improved by 6.5% in polysulfone Udel® 3500-P and 7.7% in polyimide Matrimid® with 32 wt.% loading. Remarkable H_2 permeability improvements of 475% and 148% were recorded for the stated MMMs, respectively. They also reported a 3-fold CO_2 permeability enhancement in the CO_2/CH_4 mixed gas separation, while the selectivity increased by 21% and 31%, respectively for Udel® 3500-P (32 wt.% UiO-66) and Matrimid® (16 wt.% UiO-66). Nik *et al.* [19] optimized 6FDA-ODA gas separation performance by incorporating 25 wt.% of the MOF. They improved the CO_2 permeability by 3.5 folds while maintaining the CO_2/CH_4 selectivity. Anjum *et al.* [21] also obtained an enhancement in membrane CO_2/CH_4 separation performance when embedding 30 wt.% UiO-66 in polyimide Matrimid®. Shen *et al.* [29] utilized polyether block amide (PEBAX MH 1657) for their CO_2/N_2 binary gas MMM and achieved the best selectivity with 7.5 wt.% UiO-66 loading. The selectivity and CO_2 permeability were improved by 31% and 73%, respectively. Higher loading addition, unfortunately, decreased the CO_2/N_2 selectivity, even to a lower performance than that of the base polymer. Several publications have been made on UiO-66 MMMs for different applications, such as pervaporation [26], nanofiltration [30] and reverse osmosis [31].

We aimed to enhance CO_2/CH_4 gas separation of low and high fluxes 6FDA-polyimides, by making MMMs with different loadings of MOF UiO-66 nanoparticles. The nanoparticles, 50, 100 and 200 nm in size, were incorporated into three types of 6FDA based copolyimides

with different aromatic diamine moieties, namely 6FDA-BisP, 6FDA-ODA and 6FDA-DAM. The chemical structures of the glassy polyimides are presented in Figure 1b – 1d.

2. Experimental

1.1. UiO-66 syntheses

The synthesis of the UiO-66 nanoparticles (ca. 50 nm in size) was conducted accordingly to the literature [32], at 1 to 1 molar ratio of zirconium (IV) chloride ($ZrCl_4$, ≥99.5% trace metal basis, Sigma-Aldrich) to benzene-1,4-dicarboxylic acid (BDC, 98%, Sigma-Aldrich) in *N,N*-dimethylformamide (DMF, ≥99.9%, Sigma-Aldrich) with a small addition of water. Commonly, 1.71 mmol (0.40 g) of $ZrCl_4$ was dissolved in 100 mL of DMF at room temperature by sonication, before the addition of equimolar BDC (0.28 g) and 6.84 mmol (0.13 mL) of distilled water. Valenzano *et al.* [24] also reported a similar strategy to control the MOF particle size, instead of using other additives such as acetic acid, hydrochloric acid and formic acid [23,29,33]. The same amount of $ZrCl_4$ and BDC were also used to prepare UiO-66 of ca. 100 nm [26] in 100 mL of DMF, with an addition of 3.0 mL of acetic acid (≥99.8, Sigma Aldrich), instead of water. Whereas for UiO-66 of ca. 200 nm, 5 mmol (1.16 g) of $ZrCl_4$ was dissolved in 150 mL of DMF, followed by the addition of 5 mmol (0.83 g) of BDC, without any additive [34]. The solution was later transferred into a stainless steel Teflon-lined autoclave for a solvothermal process in a pre-heated oven at 120 °C for 24 h. After cooling to room temperature, the colloidal suspension was centrifuged at 10,000 rpm for 15 min. The precipitated MOF was rinsed with 25 mL of fresh DMF for three times, followed by washing with the same amount of methanol three times. For each washing step, the suspension was subjected to sonication for 2 – 3 min to re-disperse the possible agglomerated nanoparticles and to allow for a solvent exchange. The MOF was activated by thermal treatment in a muffled furnace at 300 °C for 3 h, with heating rates of 15 °C·min^{-1}.

1.2. 6FDA-BisP and 6FDA-ODA syntheses

We followed a classic two-step polymerization method by condensation, where one-to-one stoichiometry amount of dianhydride and diamine monomers were reacted in a polar aprotic solvent under N_2 atmosphere to produce poly(amic) acid (PAA) solution. A PAA solution of 10 wt.% polymer concentration was made by first dissolving the diamine, followed by addition of the dianhydride. The obtained PAA was thermally annealed at 70 – 250 ºC for 6FDA-BisP and 70 – 300 °C for 6FDA-ODA. The first annealing step was conducted at 70 ºC overnight, followed by a gradual temperature increment (50 ºC/h) before maintaining at the highest temperature for 2 hours before cooling. The synthesis of 6FDA-ODA was conducted using 9 mmol (4.0 g) of 4,4'-(hexafluoroisopropylidene) diphthalic anhydride (6FDA, 99%, Sigma-Aldrich), 9 mmol (1.8 g) of 4,4′-oxydianiline (ODA, 97%, Sigma-Aldrich) in 58 g of DMF. Additional detail procedures for the polymer synthesis can be found elsewhere [35,36].

Whereas for 6FDA-BisP, 10 mmol (4.5 g) of 6FDA and 10 mmol (3.5 g) of 4,4′-(1,4-phenylenediisopropylidene) bisaniline (BisP, ≥99%, Mitsui, Japan) were mixed in 72 g of *N*-methyl-2-pyrrolidinone (NMP, ≥99%, Merck). The dianhydride was dried prior to the synthesis by vacuum drying at 160 °C for 6 – 7 h to discard moisture in the monomer, while the diamine was used as received. Finally, 6FDA-DAM (Mw = 418,000) was purchased from Akron Polymer Systems, Inc, and dried overnight at 100 ºC before use.

1.3. Membrane fabrication

Pure polymer membranes and MMMs were both fabricated by dissolving the corresponding amount of polyimide in chloroform, making a dope solution of 10 wt.%. For the MMMs, a pre-weighed amount of the UiO-66 nanoparticles was first re-dispersed in the

chloroform under sonication for 2 h. To create a better filler-polymer interaction and thus produce an MMM with an optimal filler dispersion and lower agglomeration [37,38], a 10 – 15% of the total amount of polyimide was added under a rigorous magnetic-stirrer mixing for priming step. The remaining polyimide was added after 4 – 5 h of the priming step and the particle loading was calculated.

$$Particle\ loading, wt.\% = \frac{Mass\ of\ filler\ (g)}{Mass\ of\ filler\ (g) + mass\ of\ polymer\ (g)} \times 100\% \qquad \text{Eq. 1}$$

The final solution was poured into a casting petri dish on a leveled surface to produce flat sheet membranes. The dense membranes were made under a controlled solvent evaporation rate overnight at room temperature, followed by a heat treatment at 180 ºC for 24 h to remove the remaining trapped solvent.

1.4. Characterizations

Scanning electron microscope (SEM), JEOL JSM 6400 operating at 20 kV was utilized to characterize the morphology of the UiO-66 crystals and the membranes. The MMMs cross-section was prepared by a freeze-fracturing method in liquid N_2. For an easier freeze-fracturing step, the membranes were first soaked in aqueous ethanol prior to immersion in the liquid N_2. UiO-66 nanoparticles were also imaged by transmission electron microscopy (TEM) using an FEI Tecnai T20 operated at 200 kV. The MOF crystals were first re-dispersed in ethanol and sonicated for a few minutes, and a couple of drops of the suspended particle solution were placed onto a holey carbon grid for the measurement.

N_2 sorption isotherms were determined using a Micromeritics Tristar 3000 porosity analyzer at -196 ºC. The specific surface area was calculated using the BET method (P/P_0 = 0.08 – 0.16). CO_2 and CH_4 isotherms were obtained using an ASAP 2050 (Micromeritics),

assessing Temkin and Freundlich adsorption in the 100 – 1000 kPa range, at 25 ºC. The samples were degassed for both methods at 100 ºC for 8 h prior to testing.

X-ray diffraction (XRD) patterns of the nanoparticles and membranes were obtained using a PANanalytical Empyrean multipurpose diffractometer (40 kV, 20 mA) with a Cu-Kα (λ = 0.1542 nm) anode from 2θ of 2.5° to 40° with a 0.03º step·s^{-1}. Thermogravimetric analysis (TGA) was conducted using a Mettler Toledo TGA/SDTA 851^{e} in the air flow of 40 mL(STP)·min^{-1} up to 750 ºC at a ramping of 10 ºC·min^{-1}. Differential scanning calorimetry (DSC) was conducted on a ca. 10 mg sample using a Mettler Toledo DSC822e system, measured in two cycles up to 450 ºC at the temperature ramping of 20 ºC·min^{-1}. ATR-FTIR was performed using a Bruker Vertex 70 spectrometer, equipped with a DTGS detector. The measurements were conducted from 600 to 4000 cm^{-1} at a resolution of 4 cm^{-1}. Both XRD and ATR-FTIR were also carried out on several MMMs to determine the MOF-polyimide chemical structure interactions.

The fractional free volume of the membranes was calculated from:

$$FFV = \frac{V - V_0}{V} = 1 - \rho V_0 \qquad \text{Eq. 2}$$

$$V_0 = 1.288 \times V_{vdw} \qquad \text{Eq. 3}$$

Where $V = 1/\rho$ is the specific volume, and V_0 is the occupied volume of the polymer at -273 ºC (Eq. 2), estimated at 1.288 times the van der Waals volume (V_{vdw}) (Eq. 3), as recently published by Horn [39]. The van der Waals volume was calculated based on the revised Bondi's group contribution method by Park and Paul [40]. The density measurement was conducted using a pycnometer (Picnomatic Thermo) at 20 °C ± 0.01 °C where ca. 100 mg of

sample was placed in the analysis cell and degassed using helium as a dry gas by a series of pressurization cycles from 2 to 20 bar.

1.5. Gas separation performance

The membranes were tested with a 50:50 (v:v) CO_2 and CH_4 binary mixture, with a feed pressure of ca. 3 bar and the sweep gas was regulated by a mass-controller (Alicat Scientific, MC-5CCM-D) to maintain a pressure difference of 2 bar at 35 ºC. A 50 cm^3 (STP)·min^{-1} feed entered the permeation module with He as sweep gas (at 0.5 cm^3 (STP)·min^{-1} for 6FDA-BisP and 6FDA-ODA membranes, and at 1 cm^3 (STP)·min^{-1} for 6FDA-DAM membranes). The membranes were sealed with a Viton® O-ring in a stainless steel permeation module equipped with a microporous disk, 316LSS of 20 µm nominal pore size (Mott Corp.) as a support in the controlled temperature oven. The permeation set up was described in an earlier publication [41]. The permeate compositions were analyzed online by an Agilent 3000A micro-GC equipped with a thermal conductivity detector (TCD).

Gas permeation through a polymer is defined by the solution-diffusion theory due to the pressure difference and concentration gradient [42]. The permeability is described as the penetrated gas flux, normalized by the membrane thickness and the partial pressure drop across the membrane, and presented in Barrer (1 Barrer = 10^{-10} cm^3(STP)·cm·cm^{-2}·s^{-1}·cm·Hg^{-1} (Eq. 4). The separation factor (α) of two competing gasses was calculated using Eq. 5, considering the mole fraction (x) of gas i and j in both feed and permeate streams.

$$Permeability, P_{gas} = \frac{Flux_{gas}\left(cm^3(STP).cm^{-2}.s^{-1}\right) \times Thickness\ (cm)}{\Delta p_{gas}\ (cm.Hg)} \quad \text{Eq. 4}$$

$$\alpha_{i/j} = \frac{x_i^{perm.}/x_j^{perm.}}{x_i^{feed}/x_j^{feed}} \quad \text{Eq. 5}$$

3. Results and discussion

1.1. Filler characterization

UiO-66 nanoparticles with size ca. 50 nm and BET surface area of 951 ± 14 $m^2 \cdot g^{-1}$, close to the accessible theoretical surface of 1021 $m^2 \cdot g^{-1}$ [22], were synthesized. Figure 2a (inserted) shows the XRD pattern of the UiO-66 in good agreement with the literature [24]. Figure 2a corresponds to the TGA characterization, where the negligible weight loss below 100 ºC is suggested to be an initial solvent loss, while the latter drop until 300 ºC is attributed to the dehydration of the $Zr_6O_4(OH)_4$ nodes to Zr_6O_6 [33]. The second drop up to 500 ºC is related to the decomposition of organic linkers before the oxidation of the zirconium into ZrO_2 [24,27]. The formula of the framework between 300 and 500 ºC is $Zr_6O_6BDC_x$. The amount of BDC ligand, *x,* present in the MOF was estimated from the subsequent weight loss, as presented by Katz *et al.* [33]in their simulation and experimental work on UiO-66 and its derivatives. In fact, the MOF showed a mass loss of 42.4 % close to the 43.3% simulated mass loss corresponding to the 4-ligand UiO-66. Figure 2b shows the crystal structure of UiO-66 containing 4 ligands, with colored spheres representing the tetrahedral (yellow) and octahedral (olive green) void regions in the framework.

FTIR spectra of the pure UiO-66 also exhibited a very small O-H stretching peak at the wavelength of 3650 – 3700 cm^{-1} (Figure S1), which indicated missing anionic BDC linkers, thus explaining the 0.9% lower mass loss in our UiO-66 compared to 4 ligands simulated for UiO-66 [33]. Unlike some UiO-66 synthesized following the conventional route using stronger acidic modulators, especially hydrochloric acid, the produced vacant sites were higher and sometimes resided by the stronger catalyst anion (chloride anion) to a certain extent [33]. Nevertheless, both FTIR and TGA findings complimented each other and suggested the presence of missing organic linkers in our UiO-66.

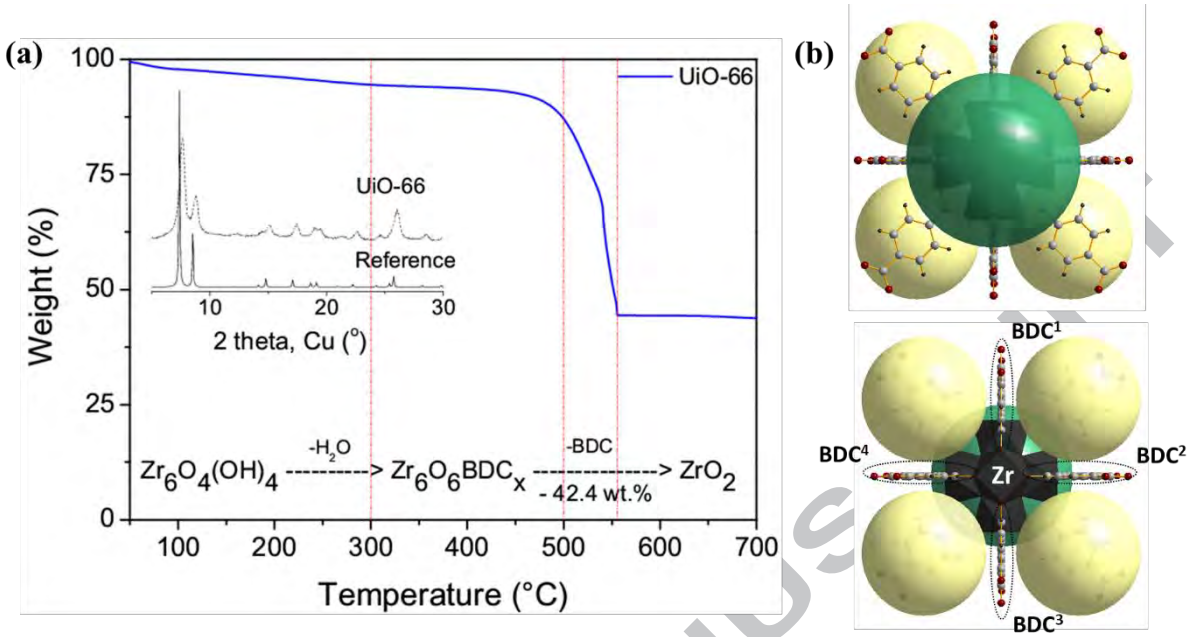

Figure 2: (a) The TGA profile of the UiO-66 nanoparticles and inserted, their XRD pattern with regards to the reference by Valenzano *et al.* [24]; and (b) the illustration of the UiO-66 crystalline structure based on a CIF on open-database CCDC [18], (Zr polyhedra, black; C, grey; O, red; and H, black).

Figures S2 and S3 display TEM and SEM images of the UiO-66 nanoparticles, respectively, after being activated at 300 ºC. The nanoparticles (ca. 50 nm) can be observed agglomerated to a certain degree, which presumably occurred during the drying process. However, individual particles are clearly visible and can be re-dispersed in highly polar solvents (i.e., ethanol) or low polarity solvents (i.e., chloroform).

Figure 3a shows the N_2 adsorption-desorption obtained from the BET analysis. N_2 adsorption analysis showed a classic type I isotherm, with the N_2 adsorbed a quantity of ca. 430 $cm^3 \cdot g^{-1}$ at P/P_o = 0.9 and -196 ºC, comparable to the recently published data [33,43]. However, a hysteresis loop can be observed after P/P_o = 0.75 due to possible capillary condensation in between the small particles. Several researchers have reported a much lower N_2 adsorption between 250 and 350 cm^3 (STP)$\cdot g^{-1}$ [23,34,44]. The N_2 adsorption behavior in the MOFs is a localized adsorption, due to N_2 quadrupole moment interaction with the MOF

monolayer polar sites; thus a lower N_2 uptake value indicates a lower cation distribution in the MOF.

The CO_2 and CH_4 adsorption capacities of the MOF display values of 1.13 and 0.28 $mmol \cdot g^{-1}$ (at 1 bar, 25 ºC), respectively (Figure 3b). Yang *et al.* [22] showed that the UiO-66 internal tetrahedral and octahedral free volumes adsorb CO_2 and CH_4 preferentially where the CO_2 had higher adsorption in the tetrahedral cages due to the CO_2 higher affinity with the framework wall. The interaction between the pore affinity and the adsorbates greatly determines the capacity of the adsorption. Table S1 indicates that the UiO-66 prepared here possess lower CO_2 and CH_4 adsorption capacities than those reported under the analogous conditions [27,34,44]. The differences are believed to be contributed by the use of different activation methods, where lower activation temperature and chemical activation produced higher adsorption UiO-66. Wu *et al.* [45] described that each hydroxylated UiO-66 framework consists of eight O-coordinated Zr ion (six of that bond together forming the $Zr_6O_4(OH)_4$ metal cluster) and losses two H_2O molecules upon full activation at high temperature (~250 °C), reducing the Zr-O coordination to seven (de-hydroxylated). They demonstrated that the hydroxylated UiO-66 adsorbed 56% more CO_2 comparing to the de-hydroxylated UiO-66 (CO_2 = 1.60 $mmol \cdot g^{-1}$). The use of syntesis modulators, i.e., acetic acid [27,45–47], benzoic acid [43,47], hydrochloric acid [48] or no modulator [19,34,44] also differed the gas adsorption properties, as the amount of missing organic linkers is influenced by the presence of the stronger anions [48]. Additionally, without modulation, Schaate *et al.* [47] presented a disordered UiO-66 phase with lower surface area comparing to those synthesized with the addition of acetic acid.

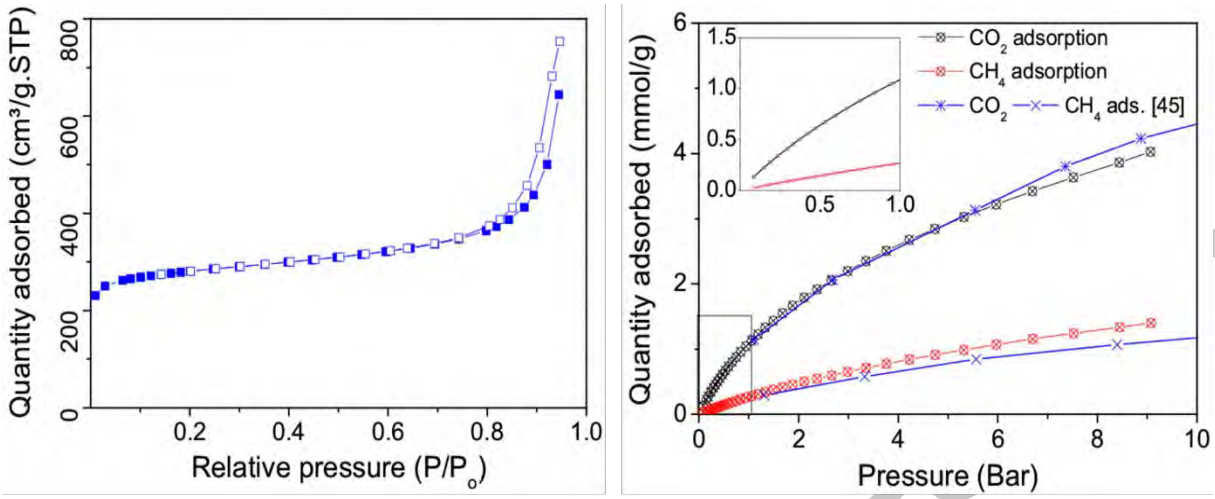

Figure 3: (a) N_2 adsorption (filled) and desorption (empty symbols) isotherms measured at -196 ºC (b) CO_2 and CH_4 isotherms, measured at 1–10 bar and 25 ºC, compared to the literature [49]. Inserted is CO_2 and CH_4 isotherms at low pressure (0.1–1.0 bar).

1.2. Membrane characterization

Thermal stabilities of MOF UiO-66 and the fabricated MMMs were characterized by TGA (Figure S4). The decomposition temperature (T_d) was obtained by the minimum of the first derivative drops and presented in Table 1. UiO-66 was stable up to 544 °C, in good agreement with reported values [25,50]. For 6FDA-BisP ($T_{d,\ pure}$ = 528 ºC), the T_d reduced gradually up to 10 ºC with 21 wt.% loading. A similar trend was observed for 6FDA-ODA ($T_{d,\ pure}$ = 545 ºC), with a reduced temperature of 13 ºC with the highest loading. However, for 6FDA-DAM ($T_{d,\ pure}$ = 523 ºC), there were no remarkable differences between all the MMMs.

Glass transition temperatures (T_g) were determined for the pure polymer membrane and the MMMs by DSC, to investigate the influence of UiO-66 addition on the polymer chain flexibility. The T_g values of all neat membranes: 6FDA-ODA, 303 ºC [19,51] and 6FDA-DAM, 396 ºC [52,53] (Table 1) were in great agreement with previously published results. Nevertheless, 6FDA-BisP, with a T_g of 383 ºC, was for the first time tested in this work. Concerning MMMs, the T_g increase was less substantial at lower loadings. However, more significant increments were observed at higher loadings. 6FDA-BisP showed a temperature increase of 14 ºC, whereas 9 ºC increment for both 6FDA-ODA and 6FDA-DAM, for their

highest loading MMMs. The T_g increase after the inclusion of the filler is usually caused by the rigidification of the polymer chain, which limits the chain movement [54]. This disruption is believed to be caused by the interface interaction created between the polymer and the inorganic moieties of the MOF. Similar observations were reported on 6FDA based co-polyimides with other MOFs, such as Noria-Co^{t}BU [53] and ZIF-11 [55].

Table 1. The T_d (decomposition temperature) and T_g (glass transition temperature) values of the neat polymer membranes and their respective MMMs.

Polymer	Particle loading (wt.%)	T_d (°C)	T_g (°C)
6FDA-BisP	0	528	383
	14	522	387
	21	518	397
6FDA-ODA	0	545	306
	8	540	311
	23	532	315
6FDA-DAM	0	523	396
	8	526	395
	21	524	405

Additionally, we conducted FTIR analysis on the samples to determine the possible chemical interaction between the MOF and the polymer matrix. Figure 4a – 4c shows the FTIR spectra obtained. The absorbance of UiO-66 is described by the strong out-of-phase carboxylic –CO– peak at 1393 cm^{-1}, and –COO– stretching (in-of-phases) at 1570 cm^{-1}, indicating its strong reaction with the zirconium. The longitudinal and transverse mode of Zr-O_2 is presented by the marked (asterisk) triplet peaks at 730, 680 and 550 cm^{-1} [20,43]. The 550 cm^{-1} peak is not shown here. Other common absorbances are at 1018 cm^{-1} for C=C aromatic stretching and the multi-peaks between 750 and 690 cm^{-1} for the di-substituted benzene ring. The FTIR absorbance for all the membranes indicated that there was no

significant shift in the key polyimide functional group signals; symmetric –C=O stretching at 1720 cm^{-1}, the imide –C-N– at 1373 cm^{-1} and also the most significant =COC= stretching at 1238 cm^{-1} in the diamine polyimide moiety of 6FDA-ODA.

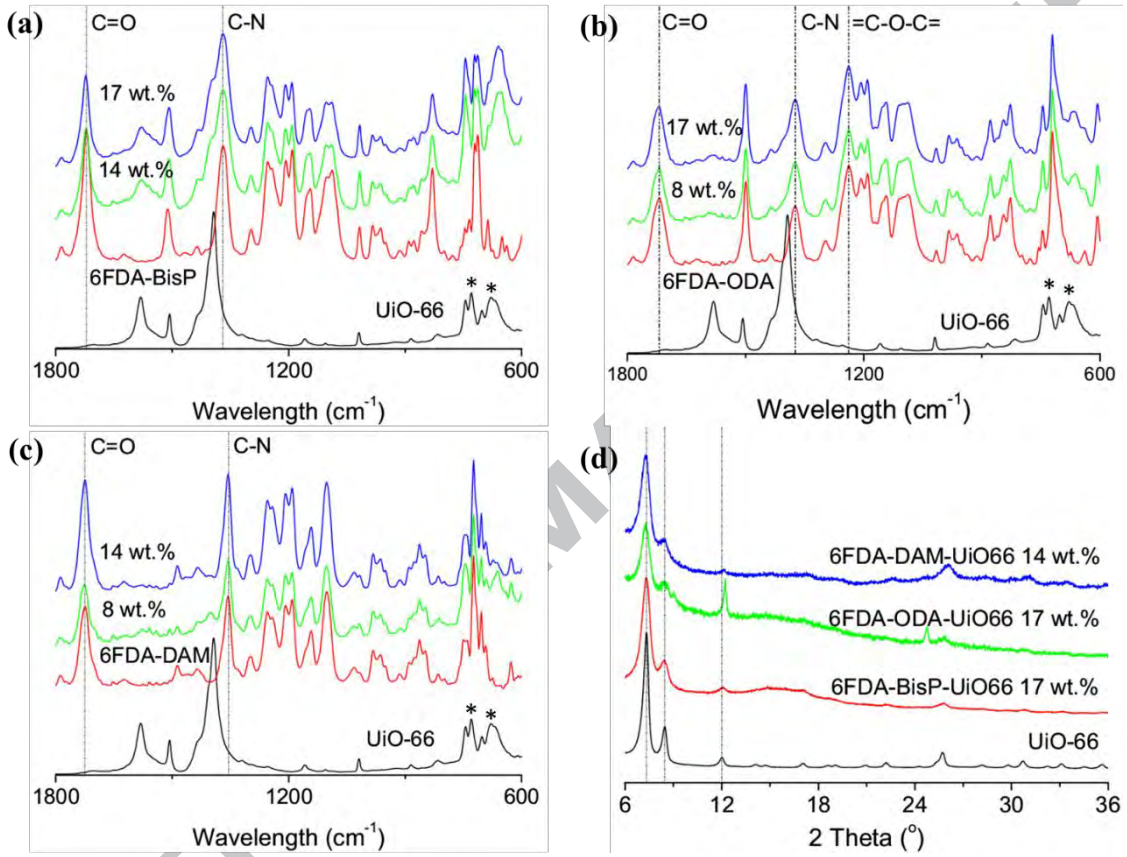

Figure 4: FTIR spectra of UiO-66, 6FDA-polyimides and their respective MMMs: (a) 6FDA-BisP, (b) 6FDA-ODA, and (c) 6FDA-DAM. The asterisk marks represent the longitudinal and transverse mode of Zr-O_2. FTIR spectrum of UiO-66 is represented for proper comparison. (d) XRD patterns of as-synthesized UiO-66 and their respective MMMs.

Figure 4c shows the XRD patterns for all MMMs, revealing that the crystalline phase of the UiO-66 was preserved in the membranes. These patterns are consistent with the afore-mentioned UiO-66 X-ray reference [24], indicated by dotted lines are some of the most critical peaks at 7.4º, 8.5º, 12.0º, corresponding to (111), (002) and (022) planes, respectively.

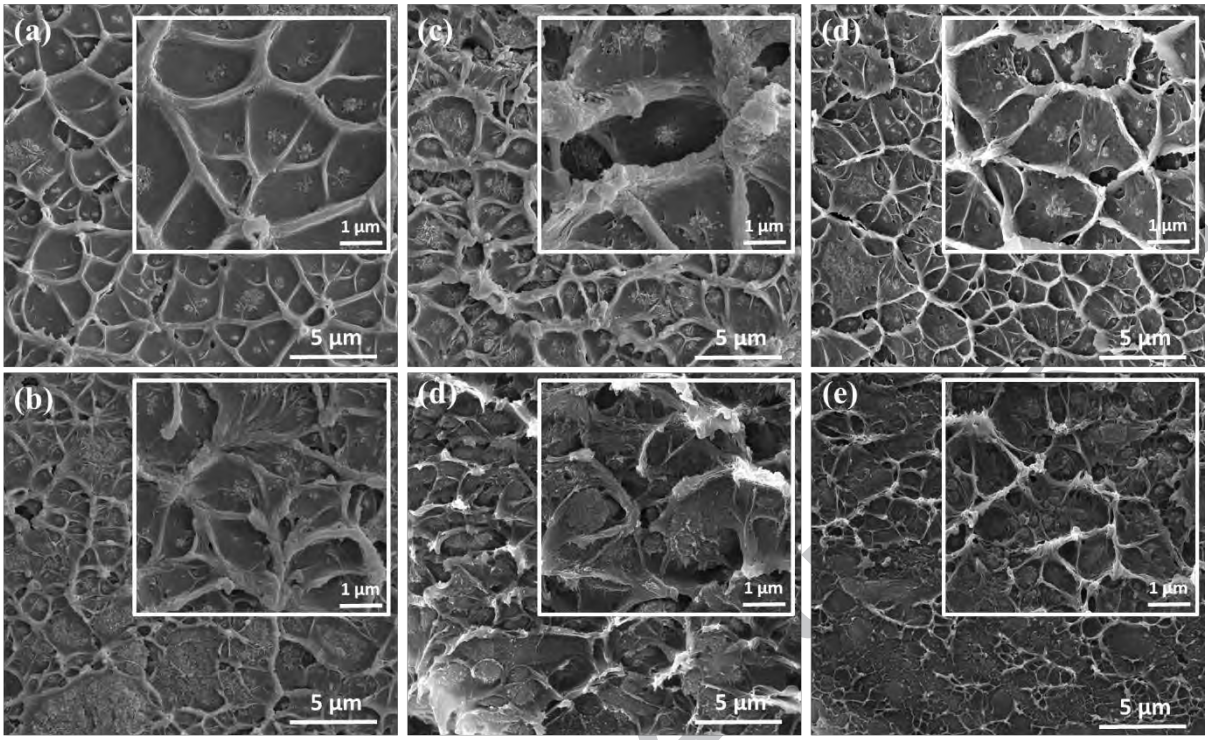

Figure 5: SEM images of the cross-sections of the mixed matrix membranes containing UiO-66 at different loadings; 6FDA-BisP with (a) 6 wt.% and (b) 14 wt.%; 6FDA-ODA at (c) 4 wt.% and (d) 17 wt.%; 6FDA-DAM with (e) 4 wt.% and (f) 14 wt.%.

The average thicknesses of the MMMs were about 30 – 60 µm for 6FDA-BisP and 6FDA-ODA and 80 – 110 µm for the 6FDA-DAM. Thinner 6FDA-BisP and 6FDA-ODA MMMs were prepared because of their lower gas permeabilities. Thus a thicker membrane required a longer stabilization period in the permeation test, comparing to the 6FDA-DAM. SEM images (Figure 5) show an excellent interface interaction between the MOF and the polymeric matrix. However, the maximum size of the particle agglomerates increased with the increment in MOF loading, from ca. 0.28 µm at the lowest loading (6 wt.%) to ca. 1.3 µm at the highest loading (21 wt.%) for 6FDA-BisP. And from ca. 0.21 µm for the lowest (4 wt.%) to 0.60 µm for the highest (21 wt.%) loading 6FDA-DAM MMMs. The agglomeration, however, was more prominent in 6FDA-ODA MMMs where the agglomerate sizes ranged up from 0.5 to 1.5 µm, between the lowest (4 wt.%) and highest (23 wt.%) UiO-66 loadings. Gas permeabilities in MMMs occur in all the three following phases: continuous

polymeric phase, the nanoparticles and the polymer-NPs interface. In the presence of NPs agglomeration, gas permeabilities may increase due to the formation of undesirable by-pass channels, connecting the voids between nanoparticles and may also reduce the membrane selectivity [10,56]. The findings with regards to our MMMs are presented in the next section.

The presence of a high number of hydrogen bond donor and acceptor in both filler and polymer structures is believed to function as an interface compatibilizer by forming hydrogen bondings. In addition to that, the presence of other functional groups which are hydrogen bond acceptor and/or donor, such as $–CF_3$ (acceptor), –C=O (donor and/or acceptor), –CO– (acceptor) and –HCN– (donor and/or acceptor) in the 6FDA-polyimides, further enhanced the intermolecular hydrogen bond. The polyimide with a higher density of H-bond promoting groups in the diamine moieties (ODA > BisP > DAM) was anticipated to have a lesser particle agglomeration, as the promoting groups may increase the MOF-polymer interaction, thus reduces the MOF-MOF interaction which leads to the agglomeration. However, the behavior was not observed, and it may be attributed to a more favorable polymer-polymer H-bonding and presumably the charge-transfer complex (CTC) phenomena in the polyimides. The CTC [57] is a type of intra- and intermolecular bond prominently occurs in aromatic polyimide membranes due to these electron acceptor/donor groups. The CTC phenomena in polyimide were exploited by many researchers in achieving higher gas-selective membranes by thermal treatment, benefiting from CTC dependence on temperature [58,59].

1.3. Gas transport properties

1.3.1. Mixed gas permeability and selectivity

Our used-as-purchased 6FDA-DAM possesses higher molecular weight (M_w = 418,000 $g \cdot mol^{-1}$; FFV = 0.24; density = 1.26 $g \cdot cm^{-3}$) comparing to the synthesized 6FDA-DAM previously tested (M_w = 81,000 $g \cdot mol^{-1}$; FFV = 0.19; density = 1.35 $g \cdot cm^{-3}$) [60]. The higher

M_w 6FDA-DAM gave rise to P_{CO2} = 997 Barrer and $\alpha_{CO2/CH4}$ = 29.2, while that of the lower M_w showed P_{CO2} = 681 Barrer and $\alpha_{CO2/CH4}$ = 21.4 [60], measured with CO_2/CH_4 equimolar feed at a pressure difference of 2 bar. The difference in the molecular weight, even though has the lesser effect on gas permeability comparing to the free volume, evidently contributed to the higher gas separation performance. Xu *et al.* [52] investigated the influence of 6FDA-DAM molecular weight for hollow fiber gas separation and presented a similar behavior. Other observations were also reported in different polymers such as polyimide Matrimid® [37]. The differences in polymer physical properties certainly influence the gas separation performance. Table 2 shows several studies on these polyimides, comparing their gas separation performances to those of our samples.

Variation in the fabrication and treatment procedures (e.g., drying temperature) of the bare membranes also affected the gas separation performance. Nik *et al.* [19] reported a two-fold higher CO_2/CH_4 selectivity for 6FDA-ODA ($\alpha_{CO2/CH4}$ = 41.7) to our neat membrane ($\alpha_{CO2/CH4}$ = 20.1), and this may be attributed to their higher annealing temperature, which usually produces a denser membrane with a lower gas permeability and higher separation factor [61].

Table 2. CO_2/CH_4 separation with pure 6FDA-polyimides with different physical properties.

Membrane	**Physical properties**			**Drying temp. (ºC)**	**Pressure difference (bar)**	**Binary gas separation performance 50:50 (vol:vol)**	
	T_g (ºC)	Density (ºC)	FFV			P_{CO2} (Barrer)	CO_2/CH_4 selectivity
6FDA-Bisp [this work*]	383	1.266	0.248	180	2	33.9	27.5
6FDA-ODA [this work]	303	1.435	0.161	180	2	25.9	20.1
[19]	294	1.455	0.169	230	10.2	14.4[a]	41.7
[51]	302	1.348	0.221	-	10	11.7	15.6
[62]	-	-	-	150	2	20.6[a]	33.1[b]
6FDA-DAM [this work]	396	1.259	0.238	180	2	997	29.2
[52]	395	-	-	-	6.9	817	17.6
[53]	383	-	-	200	1	426[a]	16.2[b]
[60]	325	1.35	0.19	180	2	681	21.4
[63]	372	1.334	0.190	382	2	299[a]	19.8
[64]	383	1.353	0.181	250	10	467[a]	15.9[b]

[a] Reported from single gas measurement; [b] Ideal selectivity; *First of this polymer for gas separation

For the three studied polymers, Table S2 and Figure 6 display the gas separation performance of the bare polymer membranes and their respective UiO-66 MMMs. Gas permeability and selectivity increased accordingly to the increase of UiO-66 loading. 6FDA-BisP MMM with 17 wt.% UiO-66 (P_{CO2} = 108 Barrer; $\alpha_{CO2/CH4}$ = 41.9) performed the best, improved by 217% and 52%, respectively, the bare 6FDA-BisP performance (P_{CO2} = 33.9 Barrer; $\alpha_{CO2/CH4}$ = 27.5). However, the further addition of UiO-66 up to 21 wt.% decreased the selectivity to 24.6 with P_{CO2} = 155 Barrer. Similar observation was found for 6FDA-ODA MMMs, where the best performing MMM was that at 17 wt.% UiO-66 loading (P_{CO2} = 43.3 Barrer; $\alpha_{CO2/CH4}$ = 57.0) with 67% and 177% increments for CO_2 permeability and CO_2/CH_4

selectivity, respectively, comparing to the bare 6FDA-ODA (P_{CO2} = 25.9 Barrer; $\alpha_{CO2/CH4}$ = 20.6). Furthermore, the membrane showed the highest CO_2/CH_4 selectivity amongst the membranes prepared in this work. However, the further addition of UiO-66 to 23 wt.% did not improve the selectivity, even though the CO_2 permeability enhanced by 66% as compared to the 17 wt.% UiO-66 loading.

6FDA-DAM MMMs showed no significant increase in the selectivity, while the CO_2 permeability increased almost to 100% with 14 wt.% UiO-66 loading (P_{CO2} = 1912 Barrer; $\alpha_{CO2/CH4}$ = 30.9) compared to the bare 6FDA-DAM (P_{CO2} = 997 Barrer; $\alpha_{CO2/CH4}$ = 29.2). Further addition of UiO-66 up to 21 wt.% increased the CO_2 permeability to 2359 Barrer with a 56% decrease in CO_2/CH_4 selectivity.

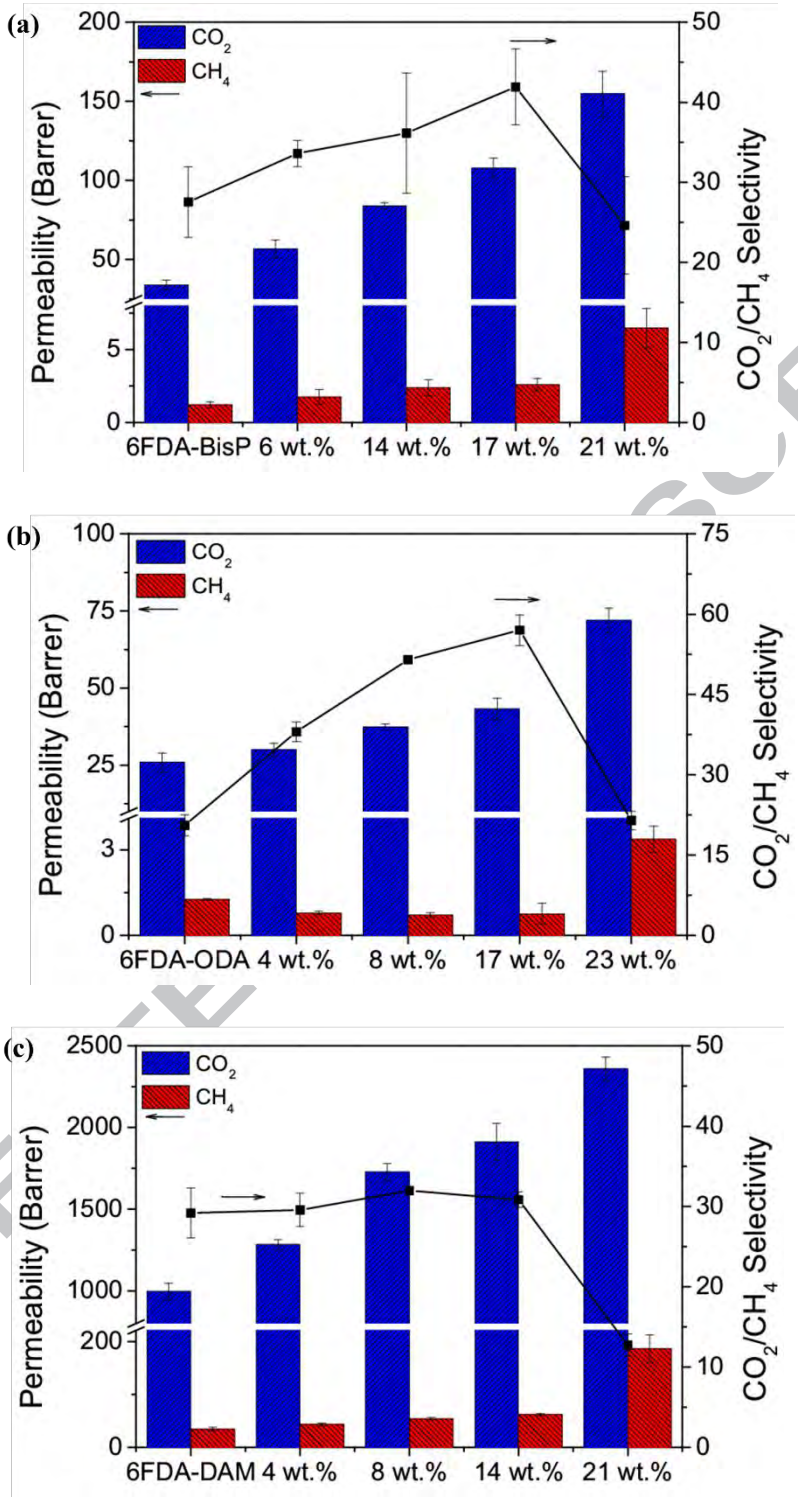

Figure 6: CO_2 and CH_4 permeabilities and CO_2/CH_4 selectivity of (a) 6FDA-BisP, (b) 6FDA-ODA and (c) 6FDA-DAM MMMs containing UiO-66 as filler, tested at 35 ºC, a pressure difference of 2 bar with an equimolar binary mixture of CO_2 and CH_4. Standards deviations were calculated based on the results of at least 2-3 different membranes, and error bars are represented accordingly.

These results suggest that the incorporation of UiO-66 nanoparticles improved both gas diffusivity and adsorption of the MMMs. Gas diffusion was enhanced through the filler-polymer interface regions [65] and the increase of the polymer free volumes [10,66,67]. The influence of FFV is discussed in the next section. The CO_2 adsorption improved significantly in all samples, ought to the CO_2-philic properties of the UiO-66 [23], in agreement with the above shown adsorption results. These findings are consistent with the previously discussed adsorption results favoring CO_2 over CH_4, and the reported higher adsorption enthalpy for CO_2 (–26.2 kJ·mol^{-1}) compared to CH_4 (–16.4 kJ·mol^{-1}) on UiO-66 [22]. It has been suggested a stronger energetic interaction between CO_2 and the UiO-66 particle surface to occur at zero coverage, supported by the fact that CO_2 has a high quadrupole moment, thus causing it to adsorb stronger on UiO-66 than CH_4. Indeed, it has been reported that UiO-66 exhibits an intrinsic CO_2/CH_4 selectivity of 5.5 – 6.9 [22,24], measured at the temperature of 25 – 50 ºC, with a 50/50 equimolar feed. Our as-synthesized UiO-66 possess a lower selectivity of 4.1, calculated with single gas at 1 bar (from data corresponding to Figure 3b). Considering the low CO_2/CH_4 selectivity and its triangular window of 6 Å as the point of gas entry, UiO-66 at a higher-than-optimum loading in polymers provided a less obstructive pathway to both CO_2 (3.3 Å) and CH_4 (3.8 Å) across the MMMs.

The optimum loadings for our 6FDA-based MMM systems were in between 14 – 17 wt.% and further addition up to 21 – 23 wt.% decreased the separation selectivity by 41 – 62%. Zornoza *et al.* [10] described how at higher loadings the polymer matrix is possibly unable to completely surround the filler particles thus producing interfacial voids, and consequently increasing the filler agglomeration. The tremendous increase in gas permeability, simultaneously reducing gas selectivity, is due to non-selective by-pass channels between the agglomerated particles [10,56] and the interfacial voids [68].

Similar observations were recently reported for CO_2/CH_4 gas pair in Matrimid® at 16 wt.%, polysulfone at 24 wt.% [12], and even at relatively low loadings especially in the highly permeable polymers, such as PIM-1 ($\alpha_{\text{bare polymer}}$ = 16.7; $\alpha_{9\text{wt.\%}}$ = 16.0) [28]. Polymer PEBA [29] produced its highest CO_2/N_2 selectivity only with 7.5 wt.% of UiO-66 loading.

Nonetheless, we further investigated the relationship between the degree of filler agglomeration and the gas separation performances by preparing additional MMMs using 6FDA-ODA with larger UiO-66 nanoparticles, at 17 and 23 wt.% loadings. The XRD patterns (Figure S5) and SEM images (Figure S6) of the ca. 100 and 200 nm nanoparticles synthesized accordingly to Xu and Chung [26] and Cao *et al.* [34] are presented, with their respective MMMs cross sections (Figures S7). It can be observed that UiO-66 ca. 100 nm were agglomerated to a higher degree than the ca. 50 nm nanoparticles. However, the ca. 200 nm nanoparticles agglomerated more prominently and produced poorer MOF-polymer interfaces. The gas performance of both MMMs with ca. 17 wt.% and ca. 23 wt.% loadings showed non-idealistic separation performances [68,69], as illustrated in Figure S8. The incorporation of ca. 17 wt.% larger UiO-66 reduced the ideally enhanced 6FDA-ODA using ca. 50 nm nanoparticles, ($\alpha_{CO2/CH4,\ 17\ wt.\%}$ = 57.0) to the ´leaking phenomenon` (represented by the formation of non-selective interface voids due to the poor filler-polymer interaction [70]), indicated by CO_2/CH_4 selectivity reductions in the 85 – 95% range. A similar ´leaking phenomenon´ was observed with the ca. 23 wt.% loading MMMs, where the selectivities were reduced by 50 – 75%, compared to the MMMs with the smallest UiO-66.

1.3.2. FFV vs. gas permeability

Figure S9 shows the CO_2 and CH_4 permeabilities of the membranes together with their respective calculated FFVs. The studied 6FDA dianhydride-polyimide showed a high free volume between 0.16 and 0.25 (6FDA-BisP = 0.248, 6FDA-ODA = 0.163 and 6FDA-DAM

= 0.238), relatively to the other dianhydride-derived polyimides (i.e. 0.12 – 0.17 for BDPA and BTDA dianhydrides, and 0.11 – 0.19 for PMDA) [71]. FFV values were similar to those previously reported [19,63], and in the higher range of the free volume values (0.1 – 0.3) of most polymers [40,67]. Gas separation of the small kinetic diameter molecules (CO_2, 3.3 Å; CH_4, 3.8 Å) in this 6FDA-polyimide membranes were governed by the diffusion mechanism. The results corresponded to the relationship of the molecule kinetic diameters with the diffusion coefficient, where the smaller molecules have higher diffusion coefficients.

In 6FDA-BisP, the increment of the FFV was observed to be the highest at 85% with 21 wt.% UiO-66 loading, and contributed to the ± 3.5-fold CO_2 permeability rise. The 17 wt.% UiO-66 MMM demonstrated the best membrane performance, having an addition of >60% FFV and produced the highest CO_2/CH_4 selectivity of 41.9. For 6FDA-DAM, a 40% increase of FFV was observed with 14 wt.% UiO-66 loading while maintaining the selectivity of 31.0. A higher FFV enhancement for 6FDA-ODA with 17 wt.% loading was achieved (FFV of 0.364), and the CO_2/CH_4 selectivity was improved to 57.0 comparing to the bare polymer (20.6). The relationship of gas permeability coefficient with FFV is presented in Figure 7, the straight lines obtained from Park and Paul correlation [40]. Both 6FDA-BisP and 6FDA-DAM behaved accordingly to the correlation. However, 6FDA-ODA did not follow the expected trend.

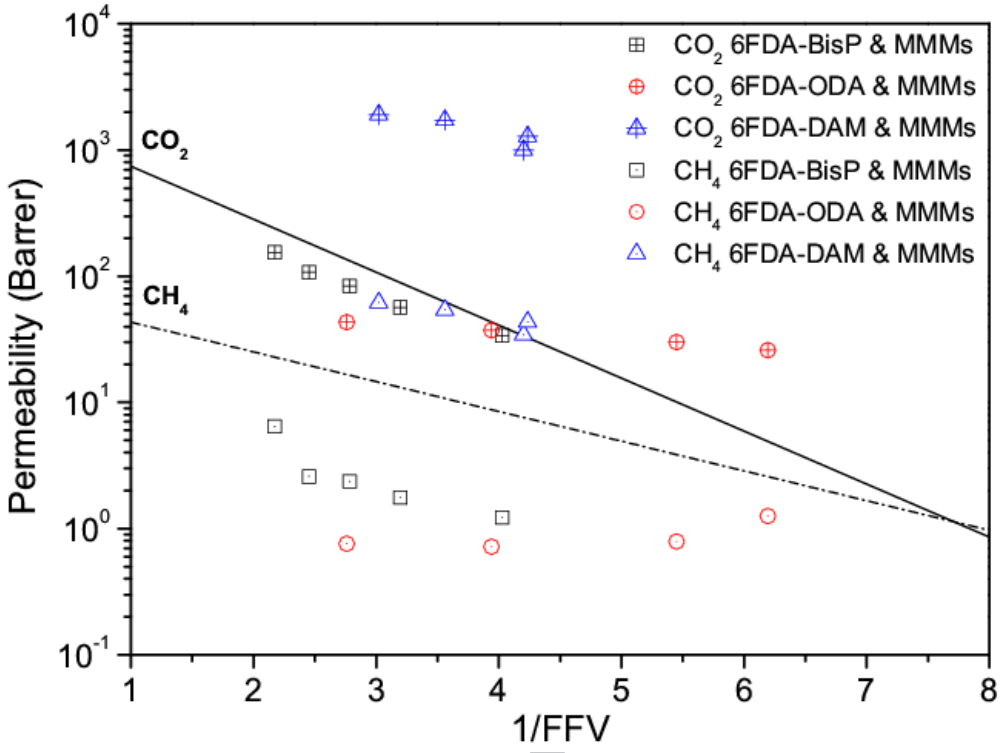

Figure 7: Gas permeability obtained against 1/FFV in comparison with CO_2 and CH_4 permeability coefficient correlations to 1/FFV by Park and Paul [40]. MMMs values were estimated using their corresponding reduced density.

In relation to the SEM images of MOF-polyimide interfaces in Figure 5, we suggested that a higher selective free volume was created in all polymer, while maintaining the ideal morphology of an MMM [70], except for MMMs with the highest loadings. At the highest loading, morphology with non-selective interface voids may have formed, as suggested from the gas selectivity reductions.

1.3.3. Performance comparisons with upper bound

Figure 8 shows the performances of all three studied 6FDA-based polyimide membranes and their MMMs with the CO_2/CH_4 1991 and 2008 Robeson upper bounds [72,73]. As depicted, 6FDA-BisP and 6FDA-ODA bare membranes resided below the upper bound. However, their respective MMMs with UiO-66 at 17 wt.% showed an improvement surpassed the 1991 upper-bound. Additional filler loading did not further improve the

CO_2/CH_4 selectivity of both membranes. The bare polymer 6FDA-DAM, however, resided above the 2008 upper-bound and further improved inward in the targeted region due to the remarkable CO_2 permeability increase, while maintaining the CO_2/CH_4 selectivity with 14 wt.% UiO-66 loading. These findings show that the UiO-66 has a good potential in MMMs for gas separation applications.

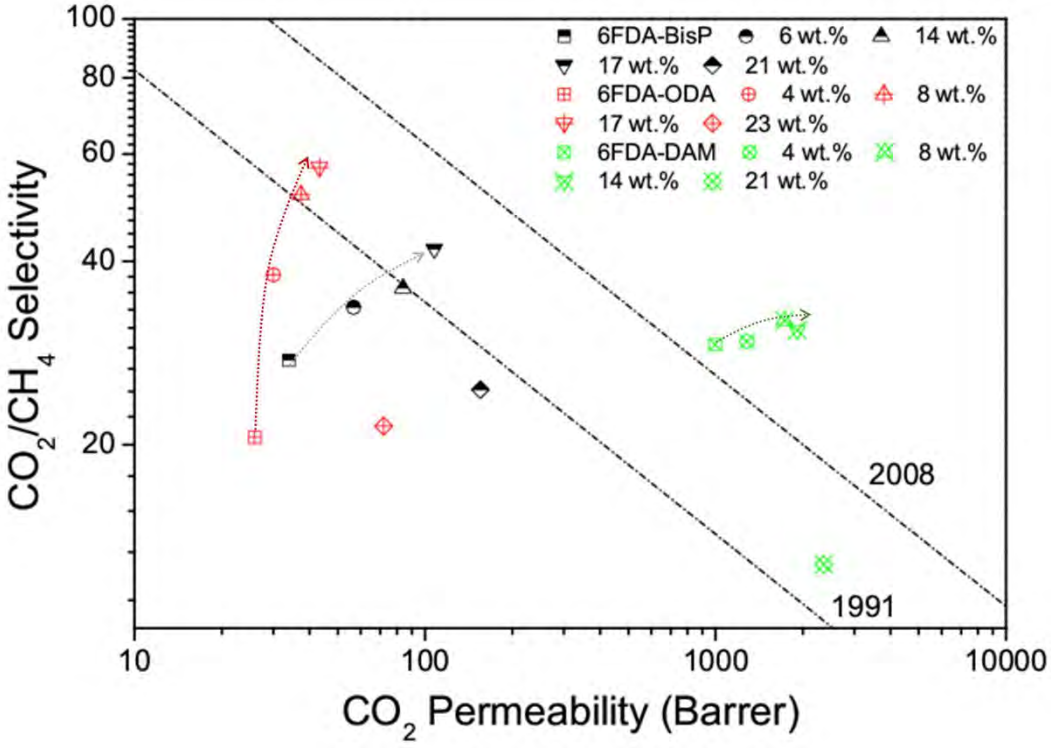

Figure 8: Separation performances of the three types of 6FDA-polyimide MMMs containing UiO-66, measured with an equimolar feed of CO_2 and CH_4 at 35 ºC, at a pressure difference of 2 bar, against 1991 [72] and 2008 [73] Robeson upper bounds.

4. Conclusion

We report the successful synthesis of high surface area Zr-based MOF UiO-66, with a uniform particle size of ca. 50 nm, appropriate crystallinity, and excellent thermal stability, as well as the fabrication of UiO-66 mixed matrix membranes with three 6FDA-based co-polyimides. Upon obtaining excellent MOF-polymer interaction with ca. 50 nm UiO-66 (and less agglomeration than using 100 and 200 nm particles), the presence of the MOF

contributed to the increase of the membrane free volumes. The gas separation performances showed significant CO_2 permeability and CO_2/CH_4 selectivity improvements. 6FDA-BisP (pristine performances of $\alpha_{CO2/CH4}$ = 27.5 ± 4.4, P_{CO2} = 33.9 ± 9.2 Barrer) were improved by 52% and 217%, while increments of 177% and 67% were obtained for 6FDA-ODA (pristine performances of $\alpha_{CO2/CH4}$ = 20.6 ± 2.0, P_{CO2} = 25.9 ± 3.0 Barrer), respectively, for selectivity and CO_2 permeability. In the case of 6FDA-DAM (pristine performances of $\alpha_{CO2/CH4}$ = 29.2 ± 3.1, P_{CO2} = 997 ± 48 Barrer), CO_2 permeability also increased by 92% while maintaining the CO_2/CH_4 selectivity. This work demonstrated that UiO-66 has the requisite advantages for fabricating mixed matrix membranes with high performance, thus making it a promising candidate for the future CO_2 capture membrane-based technologies.

Acknowledgements

The authors acknowledge the financial support of EACEA/European Commission, within the "Erasmus Mundus Doctorate in Membrane Engineering – EUDIME" (ERASMUS MUNDUS Programme 2009-2013, FPA n. 2011-0014, SGA n. 2012-1719), Operational Programme Prague – Competitiveness (CZ.2.16/3.1.00/24501), "National Program of Sustainability" of Czech Republic, (NPU I LO1613) MSMT-43760/2015 and (MAT2016-77290-R) from the Spanish MINECO and FEDER, the Aragón Government (DGA, T05) and the European Social Fund. The microscopy work was carried out in the Laboratorio de Microscopías Avanzadas at the Instituto de Nanociencia de Aragón (LMA-INA, Universidad de Zaragoza). The authors would like to acknowledge the use of the Servicio General de Apoyo a la Investigación-SAI (Universidad de Zaragoza).

References:

[1] O.M. Yaghi, M. O'Keeffe, N.W. Ockwig, H.K. Chae, M. Eddaoudi, J. Kim, Reticular synthesis and the design of new materials, Nature. 423 (2003) 705–714. doi:10.1038/nature01650.

[2] G. Férey, Hybrid porous solids: past, present, future, Chem. Soc. Rev. 37 (2008) 191–214. doi:10.1039/B618320B.

[3] X. Yan, S. Komarneni, Z. Zhang, Z. Yan, Extremely enhanced CO2 uptake by HKUST-1 metal-organic framework via a simple chemical treatment, Microporous Mesoporous Mater. 183 (2014) 69–73. doi:10.1016/j.micromeso.2013.09.009.

[4] A.R. Millward, O.M. Yaghi, Metal-organic frameworks with exceptionally high capacity for storage of carbon dioxide at room temperature, J. Am. Chem. Soc. 127 (2005) 17998–17999. doi:10.1021/ja0570032.

[5] P.L. Llewellyn, S. Bourrelly, C. Serre, A. Vimont, M. Daturi, L. Hamon, G. De Weireld, J. Chang, D. Hong, Y.K. Hwang, S.H. Jhung, High Uptakes of CO 2 and CH 4 in Mesoporous MetalsOrganic Frameworks MIL-100 and MIL-101, Langmuir. (2008) 7245–7250. doi:10.1021/la800227x.

[6] M. Montazerolghaem, S.F. Aghamiri, M.R. Talaie, S. Tangestaninejad, A comparative investigation of CO2 adsorption on powder and pellet forms of MIL-101, J. Taiwan Inst. Chem. Eng. 72 (2017) 45–52. doi:10.1016/j.jtice.2016.12.037.

[7] E. Adatoz, A.K. Avci, S. Keskin, Opportunities and challenges of MOF-based membranes in gas separations, Sep. Purif. Technol. 152 (2015) 207–237. doi:10.1016/j.seppur.2015.08.020.

[8] S.R. Venna, M.A. Carreon, Metal organic framework membranes for carbon dioxide separation, Chem. Eng. Sci. 124 (2015) 3–19. doi:10.1016/j.ces.2014.10.007.

[9] B. Seoane, J. Coronas, I. Gascon, M.E. Benavides, O. Karvan, J. Caro, F. Kapteijn, J. Gascon, Metal–organic framework based mixed matrix membranes: a solution for highly efficient CO 2 capture?, Chem. Soc. Rev. 44 (2015) 2421–2454. doi:10.1039/C4CS00437J.

[10] B. Zornoza, C. Tellez, J. Coronas, J. Gascon, F. Kapteijn, Metal organic framework based mixed matrix membranes: An increasingly important field of research with a large application potential, Microporous Mesoporous Mater. 166 (2013) 67–78. doi:10.1016/j.micromeso.2012.03.012.

[11] J.R. Long, O.M. Yaghi, The pervasive chemistry of metal-organic frameworks., Chem. Soc. Rev. 38 (2009) 1213–1214. doi:10.1039/b903811f.

[12] S. Castarlenas, C. Tellez, J. Coronas, Gas separation with mixed matrix membranes obtained from MOF UiO-66-graphite oxide hybrids, J. Memb. Sci. 526 (2017) 205–211. doi:10.1016/j.memsci.2016.12.041.

[13] J. Ahmad, M.B. Hågg, Polyvinyl acetate/titanium dioxide nanocomposite membranes for gas

separation, J. Memb. Sci. 445 (2013) 200–210. doi:10.1016/j.memsci.2013.04.052.

[14] T. Yang, T.-S. Chung, High performance ZIF-8/PBI nano-composite membranes for high temperature hydrogen separation consisting of carbon monoxide and water vapor, Int. J. Hydrogen Energy. 38 (2013) 229–239. doi:10.1016/j.ijhydene.2012.10.045.

[15] H. Yin, C.Y. Lau, M. Rozowski, C. Howard, Y. Xu, T. Lai, M.E. Dose, R.P. Lively, M.L. Lind, Free-standing ZIF-71/PDMS nanocomposite membranes for the recovery of ethanol and 1-butanol from water through pervaporation, J. Memb. Sci. 529 (2017) 286–292. doi:10.1016/j.memsci.2017.02.006.

[16] C. Zhang, Y. Dai, J.R. Johnson, O. Karvan, W.J. Koros, High performance ZIF-8/6FDA-DAM mixed matrix membrane for propylene/propane separations, J. Memb. Sci. 389 (2012) 34–42. doi:10.1016/j.memsci.2011.10.003.

[17] R. Mueller, V. Hariharan, C. Zhang, R. Lively, S. Vasenkov, Relationship between mixed and pure gas self-diffusion for ethane and ethene in ZIF-8/6FDA-DAM mixed-matrix membrane by pulsed field gradient NMR, J. Memb. Sci. 499 (2016) 12–19. doi:10.1016/j.memsci.2015.10.036.

[18] S. Øien, D. Wragg, H. Reinsch, S. Svelle, S. Bordiga, C. Lamberti, K.P. Lillerud, Detailed structure analysis of atomic positions and defects in zirconium metal-organic frameworks, Cryst. Growth Des. 14 (2014) 5370–5372. doi:10.1021/cg501386j.

[19] O.G. Nik, X.Y. Chen, S. Kaliaguine, Functionalized metal organic framework-polyimide mixed matrix membranes for CO 2/CH 4 separation, J. Memb. Sci. 413–414 (2012) 48–61. doi:10.1016/j.memsci.2012.04.003.

[20] S.J. Garibay, S.M. Cohen, Isoreticular synthesis and modification of frameworks with the UiO-66 topology., Chem. Commun. (Camb). 46 (2010) 7700–2. doi:10.1039/c0cc02990d.

[21] M.W. Anjum, F. Vermoortele, A.L. Khan, B. Bueken, D.E. De Vos, I.F.J. Vankelecom, Modulated UiO-66-Based Mixed-Matrix Membranes for CO2 Separation, ACS Appl. Mater. Interfaces. 7 (2015) 25193–25201. doi:10.1021/acsami.5b08964.

[22] Q. Yang, A.D. Wiersum, H. Jobic, V. Guillerm, C. Serre, P.L. Llewellyn, G. Maurin, Understanding the thermodynamic and kinetic behavior of the CO 2/CH4 gas mixture within the porous zirconium terephthalate UiO-66(Zr): A joint experimental and modeling approach, J. Phys. Chem. C. 115 (2011) 13768–13774. doi:10.1021/jp202633t.

[23] S. Biswas, P. Van Der Voort, A general strategy for the synthesis of functionalised UiO-66 frameworks: Characterisation, stability and CO2 adsorption properties, Eur. J. Inorg. Chem. (2013) 2154–2160. doi:10.1002/ejic.201201228.

[24] L. Valenzano, B. Civalleri, S. Chavan, S. Bordiga, M.H. Nilsen, S. Jakobsen, K.P. Lillerud, C. Lamberti, Disclosing the complex structure of UiO-66 metal organic framework: A synergic combination of experiment and theory, Chem. Mater. 23 (2011) 1700–1718. doi:10.1021/cm1022882.

[25] J.H. Cavka, S. Jakobsen, U. Olsbye, N. Guillou, C. Lamberti, S. Bordiga, K.P. Lillerud, A New Zirconium Inorganic Building Brick Forming Metal Organic Frameworks with Exceptional Stability - Journal of the American Chemical Society (ACS Publications), 6 (2008) 13850–13851. doi:10.1021/ja8057953.

[26] Y.M. Xu, T.S. Chung, High-performance UiO-66/polyimide mixed matrix membranes for ethanol, isopropanol and n-butanol dehydration via pervaporation, J. Memb. Sci. 531 (2017) 16–26. doi:10.1016/j.memsci.2017.02.041.

[27] G.E. Cmarik, M. Kim, S.M. Cohen, K.S. Walton, Tuning the adsorption properties of uio-66 via ligand functionalization, Langmuir. 28 (2012) 15606–15613. doi:10.1021/la3035352.

[28] M.R. Khdhayyer, E. Esposito, A. Fuoco, M. Monteleone, L. Giorno, J.C. Jansen, M.P. Attfield, P.M. Budd, Mixed matrix membranes based on UiO-66 MOFs in the polymer of intrinsic microporosity PIM-1, Sep. Purif. Technol. 173 (2017) 304–313. doi:10.1016/j.seppur.2016.09.036.

[29] J. Shen, G. Liu, K. Huang, Q. Li, K. Guan, Y. Li, W. Jin, UiO-66-polyether block amide mixed matrix membranes for CO2 separation, J. Memb. Sci. 513 (2016) 155–165. doi:10.1016/j.memsci.2016.04.045.

[30] D.X. Trinh, T.P.N. Tran, T. Taniike, Fabrication of new composite membrane filled with UiO-66 nanoparticles and its application to nanofiltration, Sep. Purif. Technol. 177 (2017) 249–256. doi:10.1016/j.seppur.2017.01.004.

[31] X. Liu, N.K. Demir, Z. Wu, K. Li, Highly Water-Stable Zirconium Metal-Organic Framework UiO-66 Membranes Supported on Alumina Hollow Fibers for Desalination, J. Am. Chem. Soc. 137 (2015) 6999–7002. doi:10.1021/jacs.5b02276.

[32] L. Hou, L. Wang, N. Zhang, Z. Xie, D. Dong, Polymer brushes on metal-organic frameworks by UV-induced photopolymerization, Polym. Chem. 7 (2016) 5828–5834. doi:10.1039/C6PY01008C.

[33] M.J. Katz, Z.J. Brown, Y.J. Colón, P.W. Siu, K. a Scheidt, R.Q. Snurr, J.T. Hupp, O.K. Farha, A facile synthesis of UiO-66, UiO-67 and their derivatives, Chem. Commun. (Camb). 49 (2013) 9449–51. doi:10.1039/c3cc46105j.

[34] Y. Cao, Y. Zhao, Z. Lv, F. Song, Q. Zhong, Preparation and enhanced CO2 adsorption capacity of UiO-66/graphene oxide composites, J. Ind. Eng. Chem. 27 (2015) 102–107. doi:10.1016/j.jiec.2014.12.021.

[35] O.G. Nik, X.Y. Chen, S. Kaliaguine, Amine-functionalized zeolite FAU/EMT-polyimide mixed matrix membranes for CO2/CH4 separation, J. Memb. Sci. 379 (2011) 468–478. doi:10.1016/j.memsci.2011.06.019.

[36] S. Xiao, R.Y.M. Huang, X. Feng, Synthetic 6FDA-ODA copolyimide membranes for gas separation and pervaporation: Functional groups and separation properties, Polymer (Guildf). 48 (2007) 5355–5368. doi:10.1016/j.polymer.2007.07.010.

[37] S. Japip, H. Wang, Y. Xiao, T.S. Chung, Highly permeable zeolitic imidazolate framework (ZIF)-71 nano-particles enhanced polyimide membranes for gas separation, J. Memb. Sci. 467 (2014) 162–174. doi:10.1016/j.memsci.2014.05.025.

[38] T. Yang, Y. Xiao, T.-S. Chung, Poly-/metal-benzimidazole nano-composite membranes for hydrogen purification, Energy Environ. Sci. 4 (2011) 4171. doi:10.1039/c1ee01324f.

[39] N.R. Horn, A critical review of free volume and occupied volume calculation methods, J. Memb. Sci. 518 (2016) 289–294. doi:10.1016/j.memsci.2016.07.014.

[40] J. Park, D.R. Paul, Correlation and Prediction of gas permeability in glassy polymer membrane materials via a modified free volume based group contribution method, J. Memb. Sci. 125 (1997) 23–39. doi:10.1016/S0376-7388(96)00061-0.

[41] F. Cacho-Bailo, B. Seoane, C. Téllez, J. Coronas, ZIF-8 continuous membrane on porous polysulfone for hydrogen separation, J. Memb. Sci. 464 (2014) 119–126. doi:10.1016/j.memsci.2014.03.070.

[42] Y. Xiao, B.T. Low, S.S. Hosseini, T.S. Chung, D.R. Paul, The strategies of molecular architecture and modification of polyimide-based membranes for CO2 removal from natural gas-A review, Prog. Polym. Sci. 34 (2009) 561–580. doi:10.1016/j.progpolymsci.2008.12.004.

[43] X. Zhu, J. Gu, Y. Wang, B. Li, Y. Li, W. Zhao, J. Shi, Inherent anchorages in UiO-66 nanoparticles for efficient capture of alendronate and its mediated release., Chem. Commun. (Camb). (2014) 8779–8782. doi:10.1039/c4cc02570a.

[44] D.H. Hong, M.P. Suh, Enhancing CO2 separation ability of a metal-organic framework by post-synthetic ligand exchange with flexible aliphatic carboxylates, Chem. - A Eur. J. 20 (2014) 426–434. doi:10.1002/chem.201303801.

[45] H. Wu, Y.S. Chua, V. Krungleviciute, M. Tyagi, P. Chen, T. Yildirim, W. Zhou, Unusual and highly tunable missing-linker defects in zirconium metal-organic framework UiO-66 and their important effects on gas adsorption, J. Am. Chem. Soc. 135 (2013) 10525–10532. doi:10.1021/ja404514r.

[46] S. Wang, W. Morris, Y. Liu, C.M. McGuirk, Y. Zhou, J.T. Hupp, O.K. Farha, C.A. Mirkin, Surface-specific functionalization of nanoscale metal-organic frameworks, Angew. Chemie - Int. Ed. 54 (2015) 14738–14742. doi:10.1002/anie.201506888.

[47] A. Schaate, P. Roy, A. Godt, J. Lippke, F. Waltz, M. Wiebcke, P. Behrens, Modulated synthesis of Zr-based metal-organic frameworks: From nano to single crystals, Chem. - A Eur. J. 17 (2011) 6643–6651. doi:10.1002/chem.201003211.

[48] M.J. Katz, Z.J. Brown, Y.J. Colón, P.W. Siu, K.A. Scheidt, R.Q. Snurr, J.T. Hupp, O.K. Farha, A facile synthesis of UiO-66, UiO-67 and their derivatives, Chem. Commun. 49 (2013) 9449. doi:10.1039/c3cc46105j.

[49] C.L. Luu, T.T. Van Nguyen, T. Nguyen, T.C. Hoang, Synthesis, characterization and adsorption ability of UiO-66-NH 2, Adv. Nat. Sci. Nanosci. Nanotechnol. 6 (2015) 25004.

doi:10.1088/2043-6262/6/2/025004.

[50] S. Xian, Y. Wu, J. Wu, X. Wang, J. Xiao, Enhanced Dynamic CO2 Adsorption Capacity and CO2/CH4 Selectivity on Polyethylenimine-Impregnated UiO-66, Ind. Eng. Chem. Res. 54 (2015) 11151–11158. doi:10.1021/acs.iecr.5b03517.

[51] S. Velioğlu, M.G. Ahunbay, S.B. Tantekin-Ersolmaz, Investigation of CO 2-induced plasticization in fluorinated polyimide membranes via molecular simulation, J. Memb. Sci. 417–418 (2012) 217–227. doi:10.1016/j.memsci.2012.06.043.

[52] L. Xu, C. Zhang, M. Rungta, W. Qiu, J. Liu, W.J. Koros, Formation of defect-free 6FDA-DAM asymmetric hollow fiber membranes for gas separations, J. Memb. Sci. 459 (2014) 223–232. doi:10.1016/j.memsci.2014.02.023.

[53] H. Mao, S. Zhang, Mixed-matrix membranes incorporated with porous shape-persistent organic cages for gas separation, J. Colloid Interface Sci. 490 (2017) 29–36. doi:10.1016/j.jcis.2016.11.023.

[54] V. Martin-Gil, A. Lopez, P. Hrabanek, R. Mallada, I.F.J. Vankelecom, V. Fila, Study of different titanosilicate (TS-1 and ETS-10) as fillers for Mixed Matrix Membranes for CO2/CH4 gas separation applications, J. Memb. Sci. 523 (2017) 24–35. doi:10.1016/j.memsci.2016.09.041.

[55] M. Safak Boroglu, A.B. Yumru, Gas separation performance of 6FDA-DAM-ZIF-11 mixed-matrix membranes for H2/CH4 and CO2/CH4 separation, Sep. Purif. Technol. 173 (2017) 269–279. doi:10.1016/j.seppur.2016.09.037.

[56] M.J.C. Ordoñez, K.J. Balkus, J.P. Ferraris, I.H. Musselman, Molecular sieving realized with ZIF-8/Matrimid?? mixed-matrix membranes, J. Memb. Sci. 361 (2010) 28–37. doi:10.1016/j.memsci.2010.06.017.

[57] H. Kawakami, M. Mikawa, S. Nagaoka, Gas transport properties in thermally cured aromatic polyimide membranes, J. Memb. Sci. 118 (1996) 223–230. doi:10.1016/0376-7388(96)00115-9.

[58] C. Zhang, P. Li, B. Cao, Decarboxylation crosslinking of polyimides with high CO2/CH4 separation performance and plasticization resistance, J. Memb. Sci. 528 (2017) 206–216. doi:10.1016/j.memsci.2017.01.008.

[59] M. Askari, T.-S. Chung, Natural gas purification and olefin/paraffin separation using thermal cross-linkable co-polyimide/ZIF-8 mixed matrix membranes, J. Memb. Sci. 444 (2013) 173–183. doi:10.1016/j.memsci.2013.05.016.

[60] B. Zornoza, C. Téllez, J. Coronas, O. Esekhile, W.J. Koros, Mixed matrix membranes based on 6FDA polyimide with silica and zeolite microsphere dispersed phases, AIChE J. 61 (2015) 4481–4490. doi:10.1002/aic.15011.

[61] F. Cacho-Bailo, G. Caro, M. Etxeberria, O. Karvan, C. Tellez, J. Coronas, MOF-polymer enhanced compatibility: post-annealed zeolite imidazolate framework membranes inside

polyimide hollow fibers, RSC Adv. (2016) 5881–5889. doi:10.1039/C5RA26076K.

[62] R. Lin, L. Ge, L. Hou, E. Strounina, V. Rudolph, Z. Zhu, Mixed matrix membranes with strengthened MOFs/polymer interfacial interaction and improved membrane performance, ACS Appl. Mater. Interfaces. 6 (2014) 5609–5618. doi:10.1021/am500081e.

[63] J.H. Kim, W.J. Koros, D.R. Paul, Effects of CO2 exposure and physical aging on the gas permeability of thin 6FDA-based polyimide membranes. Part 1. Without crosslinking, J. Memb. Sci. 282 (2006) 21–31. doi:10.1016/j.memsci.2006.05.004.

[64] C.K. Yeom, J.M. Lee, Y.T. Hong, K.Y. Choi, S.C. Kim, Analysis of permeation transients of pure gases through dense polymeric membranes measured by a new permeation apparatus, J. Memb. Sci. 166 (2000) 71–83. doi:10.1016/S0376-7388(99)00252-5.

[65] S. Shahid, K. Nijmeijer, Performance and plasticization behavior of polymer-MOF membranes for gas separation at elevated pressures, J. Memb. Sci. 470 (2014) 166–177. doi:10.1016/j.memsci.2014.07.034.

[66] M. Moaddeb, W.J. Koros, Gas transport properties of thin polymeric membranes in the presence of silicon dioxide particles, J. Memb. Sci. 125 (1997) 143–163. doi:10.1016/S0376-7388(96)00251-7.

[67] H. Lin, M. Yavari, Upper bound of polymeric membranes for mixed-gas CO2/CH4 separations, J. Memb. Sci. 475 (2015) 101–109. doi:10.1016/j.memsci.2014.10.007.

[68] S.A. Hashemifard, A.F. Ismail, T. Matsuura, Prediction of gas permeability in mixed matrix membranes using theoretical models, J. Memb. Sci. 347 (2010) 53–61. doi:10.1016/j.memsci.2009.10.005.

[69] K.W. Moore TT, Mahajan R, Vu DQ, Hybrid membrane materials comprising organic polymers with rigid dispersed phases. 2004;50:311–21., AIChE J. 50 (2004) 311–21.

[70] T.S. Chung, L.Y. Jiang, Y. Li, S. Kulprathipanja, Mixed matrix membranes (MMMs) comprising organic polymers with dispersed inorganic fillers for gas separation, Prog. Polym. Sci. 32 (2007) 483–507. doi:10.1016/j.progpolymsci.2007.01.008.

[71] M.L. Cecopieri-Gómez, J. Palacios-Alquisira, J.M. Domínguez, On the limits of gas separation in CO2/CH4, N2/CH4 and CO2/N2 binary mixtures using polyimide membranes, J. Memb. Sci. 293 (2007) 53–65. doi:10.1016/j.memsci.2007.01.034.

[72] L.M. Robeson, Correlation of separation factor versus permeability for polymeric membranes, J. Memb. Sci. 62 (1991) 165–185. doi:10.1016/0376-7388(91)80060-J.

[73] L.M. Robeson, The upper bound revisited, J. Memb. Sci. 320 (2008) 390–400. doi:10.1016/j.memsci.2008.04.030.

Highlights

Metal-organic frameworks (MOFs) incorporation into mixed matrix membranes (MMMs) is gaining more attention due to the combined advantages of high separation performance and easy processability. Nanoparticles (NPs) of CO_2-philic zirconium MOF UiO-66 (Zr-BDC) were synthesized with high surface area and ca. 50 nm particle size (and also for comparison with 100 and 200 nm sizes). They were incorporated into three 6FDA-based co-polyimides (namely 6FDA-BisP, 6FDA-ODA, and 6FDA-DAM), forming MMMs with loadings between 4 – 23 wt. %. The NPs and MMMs were characterized accordingly by XRD, BET, SEM, TEM, FTIR, and TGA. CO_2 and CH_4 isotherms on the NPs were measured by a static volumetric method at the pressure up to 10 bar. Fractional free volume (FFV) was calculated using solid density, measured by pycnometer. Gas separation performance was evaluated using a feed composition of 50%:50% CO_2:CH_4 binary mixture at 35 °C and a pressure difference of 2 bar. The presence of UiO-66 NPs in the continuous 6FDA-BisP and 6FDA-ODA co-polyimides improved both CO_2 permeability and CO_2/CH_4 selectivity by 50 – 180% and 70 - 220%, respectively. In the case of 6FDA-DAM MMMs, the CO_2 permeability was significantly improved by 92%, while maintaining the CO_2/CH_4 selectivity. The best results in terms of CO_2/CH_4 selectivity were 41.9 for 6FDA-BisP (17 wt.% filler loading, 108 Barrer of CO_2), 57.0 for 6FDA-ODA (7 wt.% filler loading, 43.3 Barrer of CO_2) and 32.0 for 6FDA-DAM (8 wt.% filler loading, 1728 Barrer of CO_2). The study confirmed the UiO-66 NPs incorporation into these co-polyimides has brought the positive improvement of the dense membranes, without jeopardizing their positive attributes.

Graphical Abstract